Rock Mech Rock Eng (2016) 49:3009–3025
DOI 10.1007/s00603-016-0987-z

ORIGINAL PAPER

Influence of Water Content on Mechanical Properties of Rock in Both Saturation and Drying Processes

Zilong Zhou[1] · Xin Cai[1] · Wenzhuo Cao[2] · Xibing Li[1] · Cheng Xiong[1]

Received: 16 December 2015 / Accepted: 18 April 2016 / Published online: 28 April 2016

Abstract Water content has a pronounced influence on the properties of rock materials, which is responsible for many rock engineering hazards, such as landslides and karst collapse. Meanwhile, water injection is also used for the prevention of some engineering disasters like rock-bursts. To comprehensively investigate the effect of water content on mechanical properties of rocks, laboratory tests were carried out on sandstone specimens with different water contents in both saturation and drying processes. The Nuclear Magnetic Resonance technique was applied to study the water distribution in specimens with variation of water contents. The servo-controlled rock mechanics testing machine and Split Hopkinson Pressure Bar technique were used to conduct both compressive and tensile tests on sandstone specimens with different water contents. From the laboratory tests, reductions of the compressive and tensile strength of sandstone under static and dynamic states in different saturation processes were observed. In the drying process, all of the saturated specimens could basically regain their mechanical properties and recover its strength as in the dry state. However, for partially saturated specimens in the saturation and drying processes, the tensile strength of specimens with the same water content was different, which could be related to different water distributions in specimens.

✉ Zilong Zhou
zlzhou@csu.edu.cn

[1] School of Resources and Safety Engineering, Central South University, Changsha, Hunan, People's Republic of China

[2] Department of Earth Science and Engineering, Royal School of Mines, Imperial College, London SW7 2AZ, UK

Keywords Static rock property · Rock dynamics · Water content · Saturation process · Drying process

List of Symbols

NMR	Nuclear magnetic resonance
RF	Radio frequency
UCS	Uni-axial compressive strength
XRD	X-ray diffraction
MTS	Material test system
LVDT	Linear variant differential transducer
SHPB	Split Hopkinson pressure bar
ISRM	International Society for Rock Mechanics
ω_w	Water content of the specimen (%)
m_w	Wet mass of the specimen (g)
m_d	Dry mass of the specimen (g)
σ_t	Tensile strength of the specimen (MPa)
P_m	Maximum value of loading force (kN)
D	Diameter of the specimen (mm)
L_s	Length of the specimen (mm)
σ_c	Compressive strength of the specimen (MPa)
ε_f	Failure strain of the specimen under uni-axial compression (%)
E	Elastic modulus of the specimen (GPa)
R^2	Coefficient of correlation
P_1	Force between the specimen and input bar (kN)
P_2	Force between the specimen and output bar (kN)
ε_I	Signal on the incident bar
ε_R	Signal on the reflected bar
ε_T	Signal on the transmitted bar
A_e	Cross sectional area of elastic bars (mm^2)
A_s	Cross sectional area of the specimen (mm^2)
C_e	Wave propagation velocity in the specimen (km/s)
E_e	Young's modulus of elastic bars (GPa)

1 Introduction

The mechanical properties of rock masses are largely affected by water. A small change of the water content could lead to significant changes in the strength and deformability of rocks, which are responsible for many rock engineering hazards, e.g., landslides usually occur after heavy rains (Iverson 2000), and groundwater inrush may lead to karst collapse (Bai et al. 2013). Recently, water injection was found to be effective in rock-burst relief and prevention (Lu et al. 2011; Song et al. 2014). These address a need to investigate the mechanical behaviors of rock with different water contents.

The mechanical properties of rocks with different water contents have been widely studied. Colback and Wild (1965) showed that the uni-axial compressive strength of saturated quartzitic sandstone could reduce up to 50 %. Broch (1974) reported uni-axial compressive strength (UCS) reductions of 33–53 % for phaneritic igneous and metamorphic rocks of low porosity (0.3–1.2 %) from dry to saturated state. Van Eeckhout and Peng (1975) studied the effect of relative humidity on the mechanical properties of a number of shales and found that with the increase of moisture content there was a reduction in the UCS and elastic modulus and an increase in Poisson's ratio. Hawkins and Mcconnell (1992) investigated the influence of water content on the strength and deformability of 35 different British sandstone rocks and proposed an empirical relationship between water content and uni-axial compressive strength. Vásárhelyi (2005) also conducted lots of experiments to investigate the effect of water saturation on static properties of rocks and obtained the relationship between different petro-physical parameters. Zhou and Zhao (2011) carried out a dynamic compressive experiment on cement mortar with different water contents, and found that the dynamic compressive strength of saturated specimens was 23 % lower than that of completely dry specimens.

However, limited studies have been conducted on the properties of rocks with different water contents. In most studies, only saturated state of specimens was considered and partial saturation state was ignored, so the mechanical behaviors of rock with different water contents have not yet been fully investigated. Water content is usually used to signify different saturation states of rock specimens. For the partially saturated states, another problem is the water distribution in specimens. For instance, for two rock specimens with the same water content, one of which is wet outside but dry in the core, and the other is just the opposite: dry outside and wet in the core. Studies are still limited regarding whether their mechanical properties are consistent. Therefore, more information about the effect of water content on the mechanical properties of rocks should be obtained.

In this study, a series of tests were conducted on sandstone specimens with different water contents during the saturation process (from dry to saturated state) and drying process (from saturated to dry state). The specific experimental details are listed as follows:

1. The water contents of specimens were determined by weighing every hour, and the water distribution in sandstone specimens with different saturation states was obtained from the nuclear magnetic resonance (NMR) measurement;
2. Static tests were carried out on sandstone with different water contents by the MTS-647 machine to determine the uni-axial compressive strength, tensile strength, elastic modulus and failure strain;
3. Impact tests on sandstone with different water contents were conducted with the Split Hopkinson pressure bar (SHPB) setup, and the dynamic strength of specimens were analyzed.

2 Rock Description and Specimen Preparation

The rock material used in this study is a fine-grained sandstone collected from Yunnan Province of China. The mineral composition of this sandstone was determined by the X-ray diffraction (XRD) technique. Table 1 shows the results of the XRD analysis, which indicates that this sandstone is mainly composed of quartz, feldspar, mica, calcite and chlorite. The clay content is less than 2 % by weight, which is negligible. The porosity of the sandstone is about 9.3 %.

All specimens were extracted from one sandstone block with high geometrical integrity and petro-graphical uniformity. They were manufactured in accordance with the standards in the ISRM suggested specification (Bieniawski and Hawkes 1978; Zhou et al. 2012). All specimens were cut into cylindrical shape with a diameter of 50 mm and polished to make the surface roughness less than 0.02 mm

Table 1 Mineral composition of sandstone specimen

Mineral composition	Content/%
Quartz	57
Feldspar	29
Mica	6
Calcite	4
Chlorite	2
Clay minerals	
Smectite	<1
Illite	<1
Kaolinite	[a]

[a] Could not be determined in these sandstone specimens

and the end surface perpendicular to its axis less than 0.001 radians.

In general, four sets of specimens were prepared, i.e., SC, ST, DC, DT. Specimens of set SC were used in static compressive tests. They had a length/diameter ratio of 2.0. Specimens of set ST, with a length/diameter ratio of 0.5, were used in static tensile tests. Specimens of set DC, with a length/diameter ratio of 1.0, were used in dynamic compressive tests. And Specimens of set DT, with a length/diameter ratio of 0.5, were used in dynamic tensile tests. All specimens were put in the laboratory with excellent ventilation for 1 month to get the dry state before tests.

For each set of specimens, two kinds of water-treatment processes were investigated: (1) saturation process, where the specimen went from dry to saturated state. (2) drying process, where the specimen went from saturated to dry state.

For each water-treatment process, four levels of water contents were designed. The detailed water content levels were determined in the following part.

3 Determination of Water Content and Distribution

3.1 Water Content Determination

In the saturation process, a dry specimen was inundated in a tank filled with purified water for 1 h, and then it was taken out and weighed. The operation was repeated every hour until the weight of the specimen remained unchanged. At this time, the specimen was considered to be saturated. The weight increase was used to determine the water content of the specimen at different times:

$$\omega_{\mathrm{w}} = \frac{m_{\mathrm{w}} - m_{\mathrm{d}}}{m_{\mathrm{d}}} \times 100\,\% \tag{1}$$

where $\omega_{\mathrm{w}}(\%)$ is the water content of the specimen, $m_{\mathrm{w}}(\mathrm{g})$ and $m_{\mathrm{d}}(\mathrm{g})$ are the wet and dry masses of the specimen, respectively.

In the drying process, a saturated specimen was placed in the laboratory with excellent ventilation. The specimen was also weighed every hour. The mass change values were used to calculate the water content as in formula (1). It is important to note that, the temperature in the laboratory was kept at a constant value of 25 °C during the whole process of specimen preparation.

Figure 1a, c show the water content of the specimen during the saturation and drying processes. Regression analysis further shows that the results could be described by logarithmic functions, which are plotted in Fig. 1b, d, respectively:

In saturation process:

$$\omega_w(t) = 1.1316 + 1.9195 \ln t \left(R^2 = 0.919\right) \tag{2}$$

In drying process:

$$\omega_w(t) = 3.3861 - 1.5899 \ln t \left(R^2 = 0.968\right). \tag{3}$$

It can be seen that a dry sandstone specimen reached saturated state after about 24 h (Fig. 1a), and a saturated specimen got air-dried after almost 100 h (Fig. 1c). And the maximum water content of the specimen could be 3.5 %. Therefore, 4 sets of water content levels, i.e., 0, 1.0, 2.0 and 3.5 %, were designed for tests.

3.2 Water Distribution Detected by the NMR Technique

Rock material has a large amount of internal particles and void structures, which affects its water saturation behaviors. Rock specimens with the same water content may have different water distribution states. This has not been seriously treated and studied before.

Recently, some new techniques make it possible to look into the inner parts of rocks. Here, a new technique named nuclear magnetic resonance (NMR) was used to investigate the water distribution of rock specimens with different water contents.

The NMR technique can detect hydrogen protons (^{1}H) and its energy states of water existing in materials. As we know, hydrogen proton is a particle with a positive charge (Fig. 2a). An external magnetic field may have effects on it and compel the hydrogen proton to change its original pole axis direction (Fig. 2b).

Figure 3 illustrates the operation procedure of a real NMR measurement, which includes several steps: (1) put the specimens within the NMR instrument. At that time, the hydrogen protons' pole axes are in random directions (Fig. 3a). (2) Exert the main magnetic field B_0 around the specimen. After that, the direction of the pole axes of hydrogen protons are aligned with the field B_0 (Fig. 3b). (3) Generate an oscillating RF (radio frequency) pulse B_1 at a specific angle (generally 90° or 180°) temporarily, which matches the hydrogen proton precession frequency and propels the hydrogen protons to tip over (Fig. 3c). (4) Turn off the RF pulse, and the directions of pole axes of hydrogen protons gradually return to that of B_0 and energy is released. In this process, a transient oscillating current called the NMR signal is generated and measured by a receiver (Fig. 3d). It is worth mentioning that only the wet region containing hydrogen protons in the rock specimen can generate NMR signals and can be identified (Edelman and Warach 1993; Buxton 2009).

With the NMR signals, the position information of water molecules can be decoded and transferred into NMR

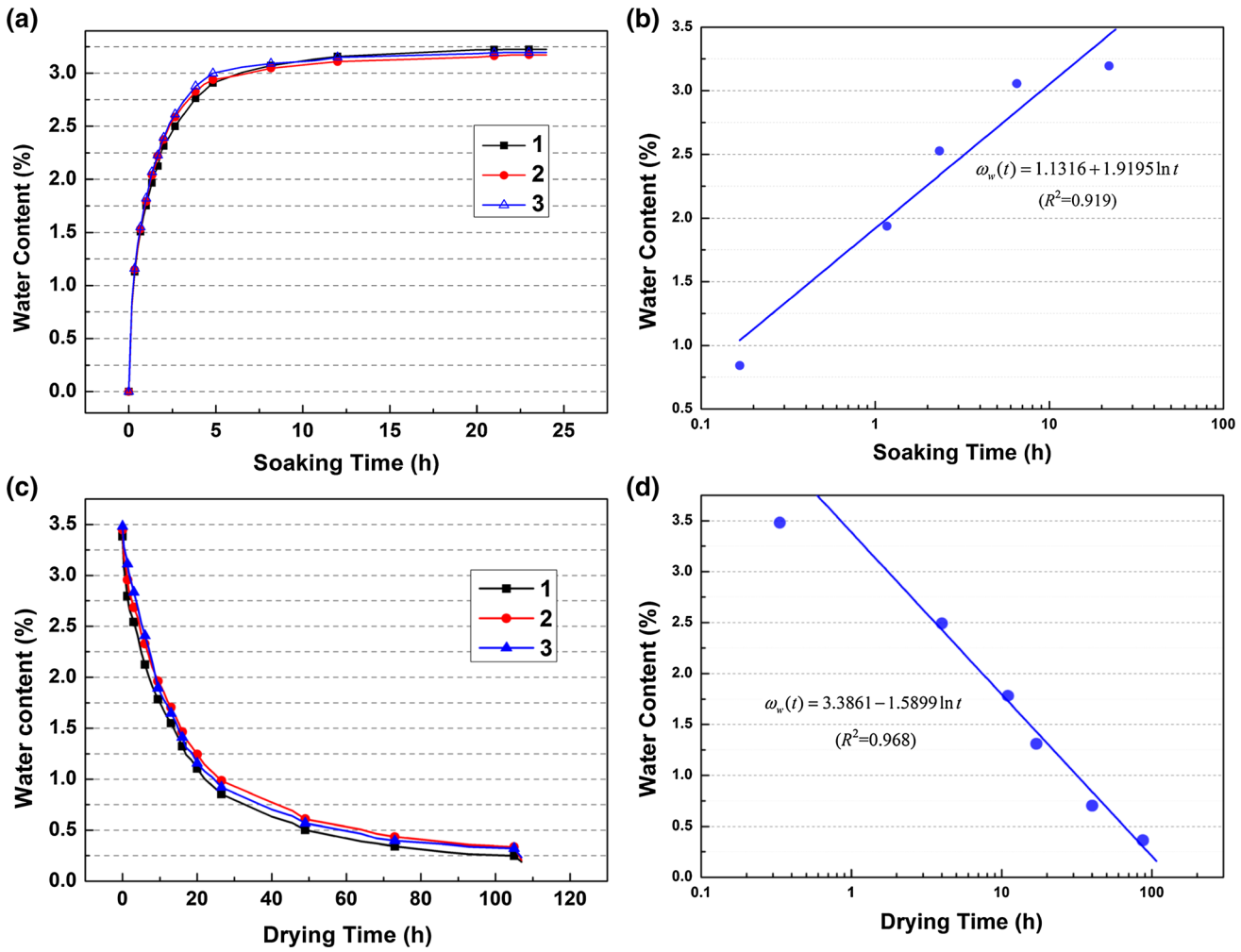

Fig. 1 Variation of water content with time for sandstone: **a** saturation process and linear coordinate; **b** saturation process and semilog coordinate; **c** drying process and linear coordinate; **d** drying process and semilog coordinate

images, and then the water distribution in rock specimens can be obtained. In this study, the MiniMR-60 (Shanghai) instrument, which is an NMR imaging and analysis system, was employed to gain the NMR images. The strength of main magnetic field is 0.51 T, the frequency of RF pulse is available between 1 and 49.9 MHz and the uniformity of magnet is 12.0 × 10^{-6}. Figure 4 gives typical NMR images of sandstone specimens. It can be seen that the NMR-images can reveal the actual water distribution in rock specimens directly, i.e., the blue points represent the water molecules existing in the specimen. The more intensive the points are, the more water molecules exist in the specimen.

3.3 Water Distribution with Different Water Contents

Tables 2 and 3 give detailed saturation states of specimens corresponding to NMR images shown in Fig. 4. It can be seen that,

1. During the process of water saturation, when the specimen began to be soaked, water only stayed on the surface and did not change the dry state of the rock core. After about 1 h, water began to soak into the rock, and gradually filled the rock pores, increasing the water content until the specimen was saturated.
2. In the initial stage of the drying process, water existed in both the inside and outside of specimens. With the increase of time, surface water gradually evaporated. After 10 h, the specimen surface was dry while the interior was still wet.
3. The process of water immersion spreads from surface to deep layers, and water evaporation also begins in the surface layer. Thus, the distribution of water in the rock is not uniform.
4. By comparing the water distribution of specimens in partially saturated states, it is obvious that although the two specimens are with the same water content, the distribution of water is quite different.

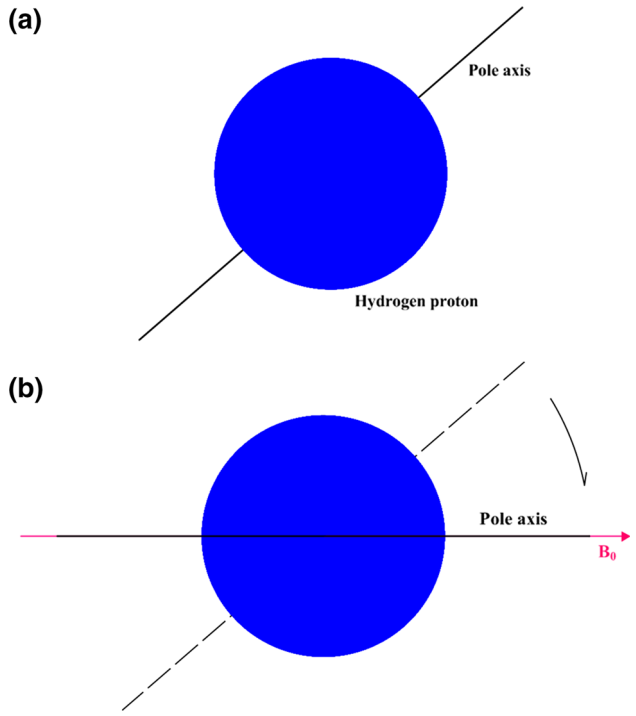

Fig. 2 Change in direction of pole axis of a hydrogen proton: **a** without magnetic field; **b** in magnetic field

4 Static Properties of Rock in Saturation and Drying Processes

4.1 Experimental Setup and Testing Methods

The static tests including compressive and tensile tests were carried out on MTS-647 in the Advanced Research Center at Central South University. MTS-647 is a servo-controlled material testing machine manufactured by the MTS Systems Corporation. It could successfully reproduce rock failure process at low and medium strain rates. The maximum vertical loading force of the testing machine is 500 kN, and the global stiffness of testing frame is about 1370 kN/mm. All tests were conducted on specimens by computerized strain control at a constant loading rate of 0.1 mm/min. During tests, the axial load was recorded by the machine directly, and the axial strain of the specimen was monitored by a linear variant differential transducer (LVDT).

The static compressive properties of specimens can be obtained directly. And the static tensile properties of specimens were obtained by the Brazilian Disc (BD) method indirectly. After tests, the tensile strength of specimens was calculated by the following formula:

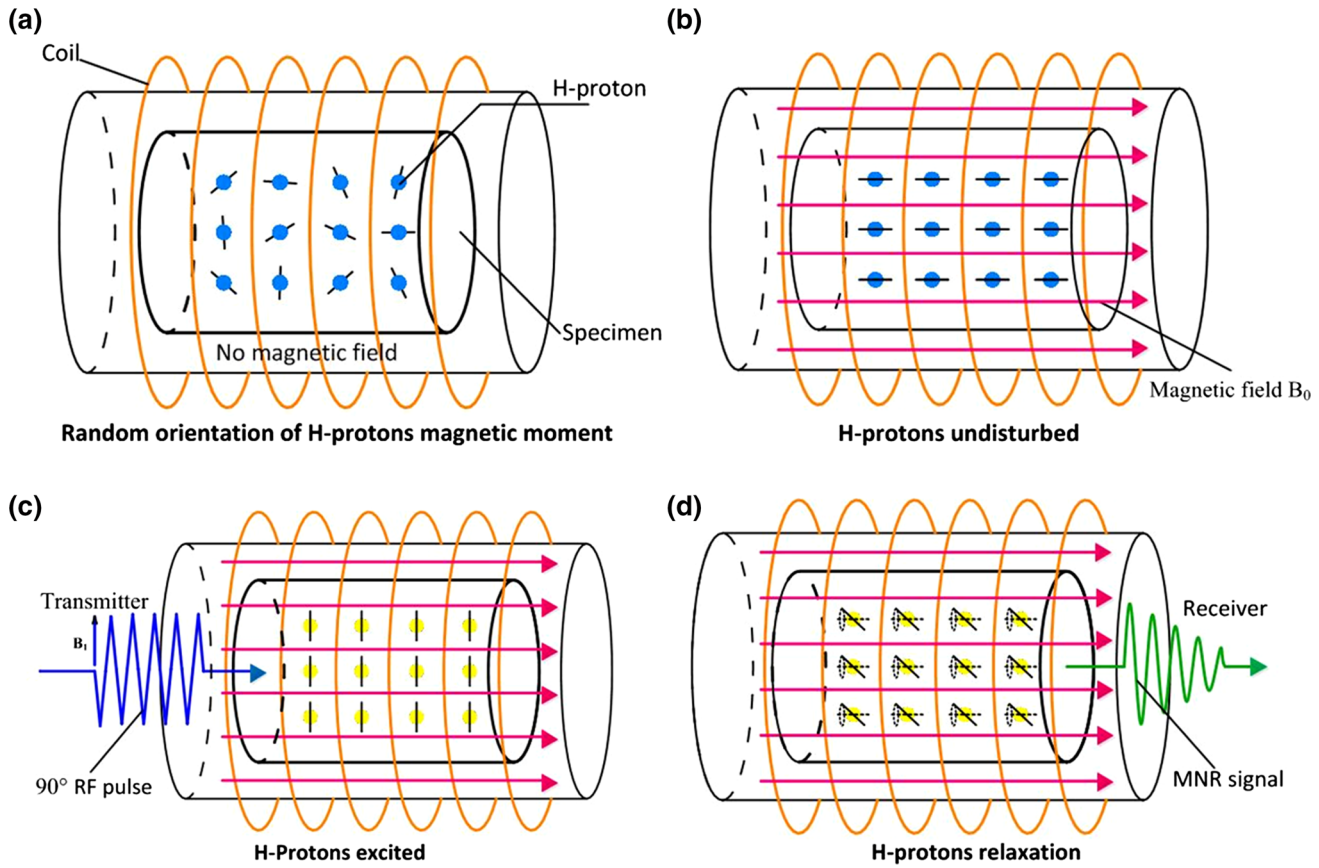

Fig. 3 Schematic of the induction of an NMR signal. **a** Natural state; **b** equilibrium state; **c** excited state; **d** spin relaxation state

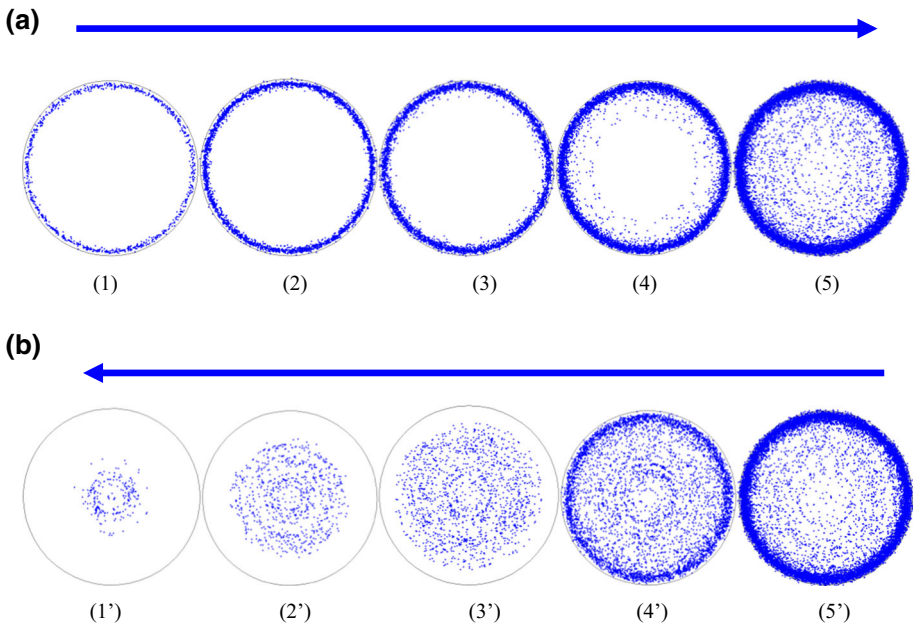

Fig. 4 NMR-images with different water contents: **a** saturation process; **b** drying process

Table 2 Saturation states of specimens corresponding to NMR images in Fig. 4a

Image no.	(1)	(2)	(3)	(4)	(5)
Soaking time/h	1/6	1/2	3	10	24
Water content/%	0.81	1.04	2.01	3.03	3.51

Table 3 Saturation states of specimens corresponding to NMR images in Fig. 4b

Image no.	(5′)	(4′)	(3′)	(2′)	(1′)
Drying time/h	0	3	10	19	24
Water content/%	3.51	3.01	1.98	1.03	0.84

$$\sigma_{\mathrm{t}} = \frac{2P_{\mathrm{m}}}{\pi D L_{\mathrm{s}}} \tag{4}$$

where σ_{t}(MPa) is the tensile strength of the specimen, P_{m} (kN) is the maximum value of loading force, D (mm) and L_{s} (mm) are the diameter and the length of the specimen, respectively.

It is important to note that the temperature of the laboratory was maintained at 25 °C during tests, to avoid the influence of temperature fluctuations on rock mechanical properties and reduce the discreteness of test results to some extent.

4.2 Static Compressive Properties of Rock with Different Water Contents

Tables 4 and 5 show the parameters of specimens with different water contents from both saturation and drying processes in the static compressive tests.

The static compressive stress–strain curves of specimens with different water contents are shown in Fig. 5. It can be seen that in compressive tests, there is an initial compaction stage when the existing micro-fissures and micropores are squeezed to close. Then the stress–strain curves are almost linear until the peak strength is reached. In general, the failure strain and elastic modulus decrease with the increase of water content for both the saturation and drying processes. At the post-peak stage, the specimen with higher water content usually experiences a less steep stress drop. This indicates that the sandstone becomes "softer" when the water content increases.

Figure 6 gives the average results of several static compressive properties of sandstone rock with different water contents. It appears that the relationship between static compressive strength and water content could be described by an exponential equation, which was brought up by Hawkins and McConnell (1992) and Vásárhelyi and Ván (2006):

$$\sigma_c(\omega_{\mathrm{w}}) = a\mathrm{e}^{-b\omega_{\mathrm{w}}} + c \tag{5}$$

where σ_c (MPa) is the compressive strength, and a, b and c are constants.

It is obvious that the compressive strength at water content of 0 is given by $\sigma_c(0) = a + c$. The parameter b is a dimensionless constant defining the strength loss rate with the increase of water content. With this analysis method, the best-fit curves are plotted in Fig. 6 and the fitting equations between water contents and the mechanical streng th are listed in Table 6.

Figure 6a further manifests that the peak strength of sandstone decreases with the increase of water content. In the saturation process, when a specimen changed from dry

Table 4 Specimen parameters in static compressive tests (saturation process)

Specimen no.	Water content/%		Density/kg m^{-3}		Strength/MPa		Failure strain/%		Elastic modulus/GPa	
	Designed	Real	Dry	Wet	Tested	Average	Tested	Average	Tested	Average
SCS1-1	0.0	0.00	2337.5	–	67.33	66.75	1.307	1.296	7.88	7.82
SCS1-2		0.00	2343.8	–	69.62		1.322		7.26	
SCS1-3		0.00	2339.1	–	64.52		1.328		7.75	
SCS1-4		0.00	2353.3	–	65.54		1.225		8.38	
SCS2-1	1.0	1.07	2351.2	2376.4	58.54	57.69	1.238	1.242	7.63	7.38
SCS2-2		1.04	2367.0	2391.6	59.53		1.202		7.32	
SCS2-3		1.08	2364.1	2389.6	56.14		1.285		7.75	
SCS2-4		1.03	2358.7	2383.1	56.55		1.242		6.81	
SCS3-1	2.0	1.95	2341.1	2386.8	52.89	51.60	1.200	1.140	6.74	6.71
SCS3-2		2.05	2331.9	2379.8	51.12		1.095		6.90	
SCS3-3		2.02	2329.1	2376.3	48.30		1.126		6.58	
SCS3-4		2.08	2330.9	2379.4	54.07		1.140		6.62	
SCS4-1	3.5	3.55	2338.0	2421.0	48.86	46.80	1.062	1.084	6.23	6.25
SCS4-2		3.43	2381.4	2463.0	44.57		1.124		6.28	
SCS4-3		3.41	2401.1	2483.1	46.99		1.121		6.17	
SCS4-4		3.44	2353.3	2434.2	46.79		1.029		6.31	

Table 5 Specimen parameters in static compressive tests (drying process)

Specimen no.	Water content/%		Density/kg m^{-3}		Strength/MPa		Failure strain/%		Elastic modulus/GPa	
	Designed	Real	Dry	Wet	Tested	Average	Tested	Average	Tested	Average
SCD1-1	3.5	3.55	2338.0	2421.0	48.86	46.21	1.062	1.087	6.31	6.20
SCD1-2		3.33	2365.9	2444.7	44.67		1.059		6.05	
SCD1-3		3.43	2381.4	2463.0	44.32		1.104		6.28	
SCD1-4		3.41	2401.1	2483.1	46.99		1.121		6.17	
SCD2-1	2.0	2.01	2329.8	2376.7	50.41	51.60	1.194	1.152	6.78	6.73
SCD2-2		2.04	2331.0	2378.6	49.11		1.114		6.61	
SCD2-3		2.14	2348.9	2399.1	54.18		1.176		6.84	
SCD2-4		2.00	2342.9	2389.9	52.71		1.124		6.69	
SCD3-1	1.0	0.99	2338.2	2361.3	58.39	58.12	1.206	1.220	7.48	7.25
SCD3-2		1.07	2352.1	2377.3	55.33		1.261		6.98	
SCD3-3		1.04	2367.0	2391.6	59.53		1.221		7.31	
SCD3-4		1.03	2333.4	2357.5	59.24		1.191		7.24	
SCD4-1	0.0	0.00	2337.5	2337.5	65.12	66.10	1.417	1.299	7.88	7.85
SCD4-2		0.08	2343.8	2345.7	68.77		1.272		7.76	
SCD4-3		0.21	2339.1	2344.0	64.02		1.293		7.65	
SCD4-4		0.18	2353.3	2357.5	66.48		1.215		8.1	

to saturated state, the average compressive strength reduced from 66.75 to 46.80 MPa, almost a 29.9 % reduction. In the drying process, when the water content declined to 0.12 %, the compressive strength of the specimen was about 66.10 MPa, which was close to that of a dry specimen.

Figure 6b, c present the variation of failure strain and elastic modulus with different water contents. It can be seen that, with the increase of water content, the failure strain and elastic modulus decrease gradually, and the maximum reduction can be 16.3 and 20.1 %, respectively. At the same time, the result curves of the saturation process and drying process do not overlap completely, which indicates the influence of water distribution. But the small difference between them in these two processes shows that the water content other than water distribution has an

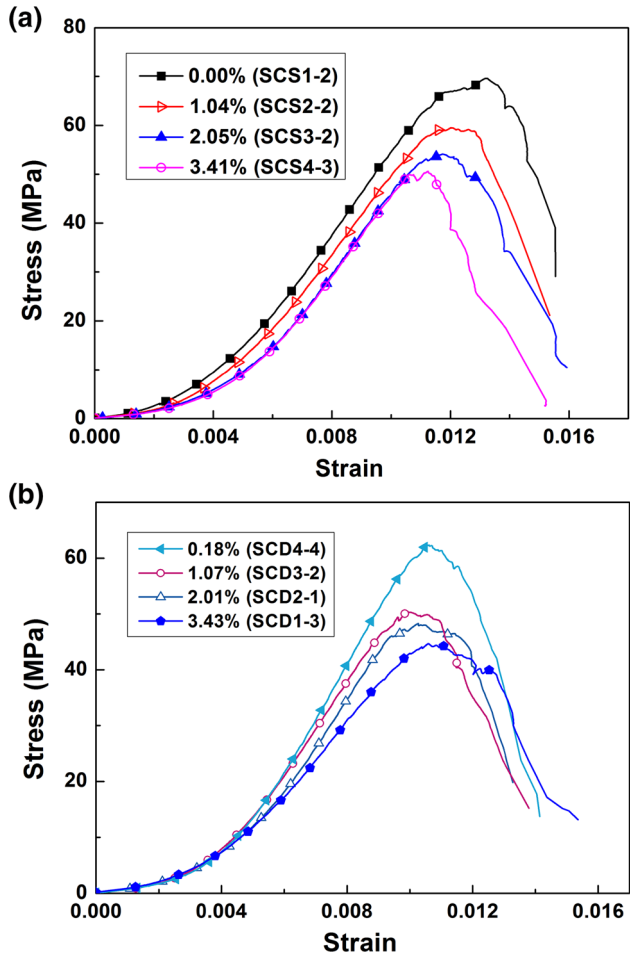

Fig. 5 Static stress–strain curves for different water contents: **a** saturation process; **b** drying process

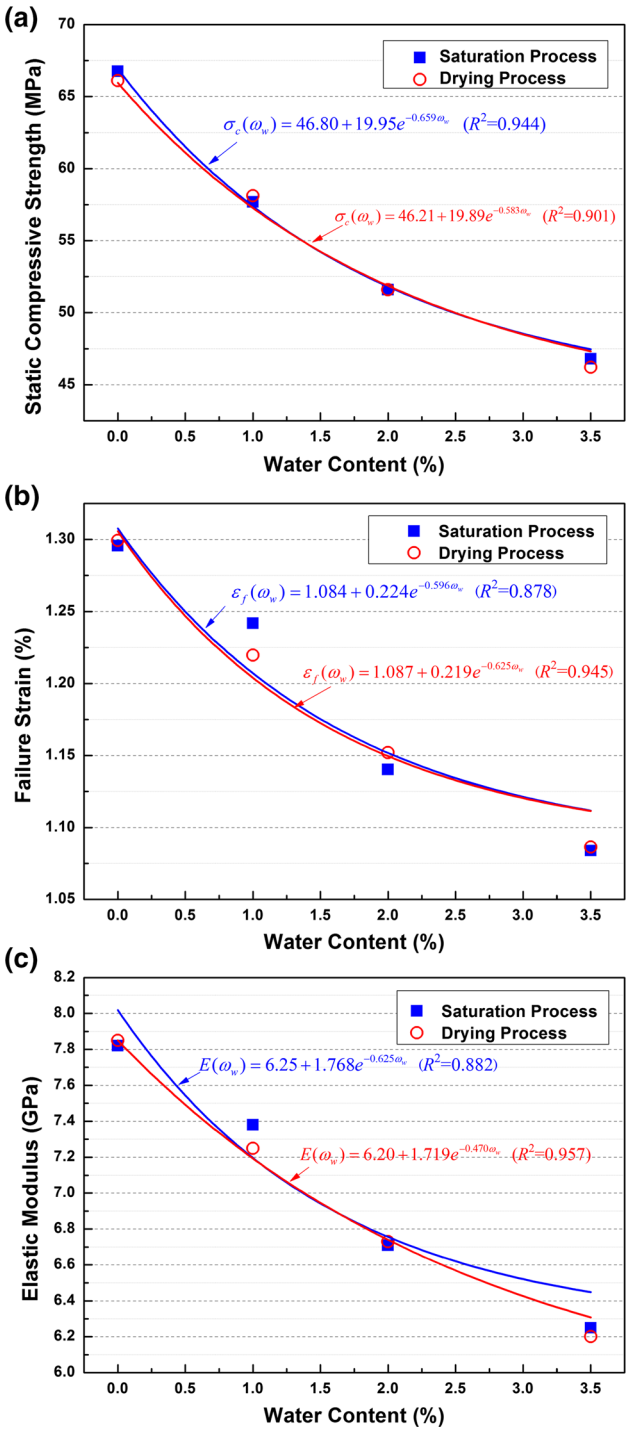

Fig. 6 Variation of static compressive properties with water content. **a** Static compressive strength; **b** failure strain; **c** elastic modulus

evident effect on the mechanical properties of rock under compressive loadings.

4.3 Static Tensile Properties of Rock with Different Water Contents

Tables 7 and 8 give the parameters of specimens with different water contents from both saturation and drying processes in the static tensile tests.

Figure 7 shows the static tensile load–displacement curves of specimens with different water contents. It can be seen that the bearing load of the BD specimen grows steadily without obvious signs of instability before it reaches the peak value. After that, the specimen loses its bearing capability abruptly, as the central failure occurs at this time according to the BD test theory.

Figure 8 further presents the variation of static tensile strength versus water content in the saturation process. It can be seen that the static tensile strength decreases with the increase of water content of specimens. When the specimen reached a water content of 3.5 %, the static tensile strength decreased to 1.15 MPa, which was 66.5 % of that of dry specimens. It can also be seen that when the water content was below 1.0 %, the tensile strength was almost unchanged.

Table 6 Correlations between the mechanical strength and water contents (R^2: coefficient of determination)

Mechanical properties	Relationship equations
Strength	In saturation process: $\sigma_c(\omega_w) = 46.80 + 19.95e^{-0.659\omega_w}$ $(R^2 = 0.944)$
	In drying process: $\sigma_c(\omega_w) = 46.21 + 19.89e^{-0.583\omega_w}$ $(R^2 = 0.901)$
Failure strain	In saturation process: $\varepsilon_f(\omega_w) = 1.084 + 0.224e^{-0.596\omega_w}$ $(R^2 = 0.878)$
	In drying process: $\varepsilon_f(\omega_w) = 1.087 + 0.219e^{-0.625\omega_w}$ $(R^2 = 0.945)$
Elastic modulus	In saturation process: $E(\omega_w) = 6.25 + 1.768e^{-0.625\omega_w}$ $(R^2 = 0.882)$
	In drying process: $E(\omega_w) = 6.20 + 1.719e^{-0.470\omega_w}$ $(R^2 = 0.957)$

Table 7 Specimen parameters in static tensile tests (saturation process)

Specimen no.	Water content/%		Density/kg m^{-3}		Strength/MPa	
	Designed	Real	Dry	Wet	Tested	Average
STS1-1	0.0	0.00	2346.2	–	1.81	1.73
STS1-2		0.00	2349.2	–	1.68	
STS1-3		0.00	2339.5	–	1.71	
STS1-4		0.00	2351.0	–	1.72	
STS2-1	1.0	1.02	2332.7	2356.5	1.74	1.70
STS2-2		0.95	2348.8	2371.1	1.64	
STS2-3		0.96	2334.0	2356.5	1.79	
STS2-4		1.13	2360.5	2387.1	1.61	
STS3-1	2.0	1.98	2345.9	2392.3	1.38	1.40
STS3-2		1.94	2331.1	2376.4	1.31	
STS3-3		2.06	2341.3	2389.6	1.47	
STS3-4		2.09	2348.8	2398.0	1.45	
STS4-1	3.5	3.44	2328.0	2403.5	1.12	1.15
STS4-2		3.36	2355.3	2434.4	1.26	
STS4-3		3.46	2332.6	2413.4	1.14	
STS4-4		3.35	2343.7	2422.3	1.08	

Figure 8 also presents results of the drying process. It is noted that the tensile strength did not vary significantly with the reduction of water content from 3.5 to 2.0 %. After that, the static tensile strength increased greatly with the decrease of water content. It also shows that when the water content reduced to 0.13 %, the static tensile strength reached 1.71 MPa, approaching that of dry specimens.

Interestingly enough, there is a significant distinction among tensile strength values of specimens with the same water content but in different processes. From Fig. 8 and Tables 7, 8, when the water content was 1.0 %, the tensile strength value of the specimen was 1.70 MPa in the saturation process, while being 1.46 MPa in the drying process. A difference of 14.1 % can be observed. When the water content was 2.0 %, the tensile strength values of the specimen in the saturation process and drying process were 1.40 and 1.16 MPa, respectively, which yielded a great difference of 20 %. This indicates that, not only water content but also water distribution would play important roles in controlling the static tensile failure of sandstone rocks.

5 Dynamic Tests and Results

5.1 SHPB Test and its Principle

Split Hopkinson pressure bar (SHPB) is a very popular and promising experimental technique for the study of dynamic material behaviors for its easy operation and relatively accurate results. Recently, it is suggested as an ISRM method for dynamic tests of rock materials (Zhou et al. 2012).

The SHPB system consists of a striker bar, an input bar, an output bar and an absorption bar. The specimen is sandwiched between the input and output bars, which are made of high strength 40Cr steel with a density of 7800 kg m^{-3}, an elastic modulus of 250 GPa and a nominal yield strength of 800 MPa. During a test, a specially shaped striker (Zhou and Zhao 2011; Zhou et al. 2011a, b) is shot out from the gas gun at a high velocity and impacts the front end of the input bar. Then an input wave is generated and propagates along the input bar towards the specimen. Once the wave reaches the bar/

Table 8 Specimen parameters in static tensile tests (drying process)

Specimen no.	Water content/%		Density/kg m^{-3}		Strength/MPa	
	Design	Test	Dry	Wet	Tested	Average
STD1-1	3.5	3.39	2365.9	2444.7	1.16	1.15
STD1-2		3.47	2381.4	2463.0	1.09	
STD1-3		3.43	2401.1	2483.1	1.18	
STD1-4		3.51	2338.0	2421.0	1.15	
STD2-1	2.0	2.03	2316.0	2363.0	1.18	1.16
STD2-2		2.12	2334.8	2384.2	1.20	
STD2-3		2.03	2257.7	2303.6	1.11	
STD2-4		2.07	2254.0	2300.6	1.16	
STD3-1	1.0	0.93	2247.9	2268.2	1.50	1.46
STD3-2		1.07	2235.2	2259.1	1.41	
STD3-3		1.01	2243.0	2265.6	1.46	
STD3-4		1.03	2258.6	2274.1	1.48	
STD4-1	0.0	0.07	2248.2	2249.8	1.71	1.71
STD4-2		0.11	2250.3	2252.8	1.74	
STD4-3		0.08	2243.0	2244.8	1.73	
STD4-4		0.04	2259.5	2260.4	1.65	

specimen interface, a part of it is reflected, whilst the remaining part goes through the specimen and transmits into the output bar. By collecting signals on the input and output bars, the dynamic parameters of the specimen can be obtained.

In Fig. 9, A_1 denotes the input bar/specimen interface and A_2 represents the specimen/output bar interface. ε represents the measured signals on the bars, where the subscripts I, R and T represent incident, reflected and transmitted pulses respectively. The arrowheads show the direction of wave propagation. According to the one-dimensional wave theory, the forces P_1 and P_2 on each end of the specimen can be calculated as:

$$P_1 = E_e A_e[\varepsilon_I(t) + \varepsilon_R(t)] \quad (6)$$

$$P_2 = E_e A_e \varepsilon_T(t) \quad (7)$$

and the relationship of the stress, strain and strain rate of the specimen can be obtained as follows (Dai et al. 2010):

$$\sigma(t) = \frac{A_e E_e}{2A_s}[\varepsilon_I(t) + \varepsilon_R(t) + \varepsilon_T(t)] \quad (8)$$

$$\varepsilon(t) = \frac{C_e}{L_s}\int_0^t [\varepsilon_I(t) - \varepsilon_R(t) - \varepsilon_T(t)]dt \quad (9)$$

$$\dot{\varepsilon}(t) = \frac{C_e}{L_s}[\varepsilon_I(t) - \varepsilon_R(t) - \varepsilon_T(t)] \quad (10)$$

where A_e, C_e and E_e are the cross sectional area (mm^2), wave velocity (km/s) and Young's modulus of elastic bars (GPa), and A_s and L_s are the cross sectional area (mm^2) and length of the specimen (mm), respectively.

Due to the rate dependence of rock materials, the strain rate must be controlled to make the strength more comparable (Zhou et al. 2010; Zhang and Zhao 2014). During tests, the impact velocity of the SHPB striker was thus regulated to ensure the strain rate was about 100 s^{-1} for all specimens.

5.2 Dynamic Compressive Properties of Rock with Different Water Contents

Tables 9 and 10 give the parameters of specimens with different water contents from both saturation and drying processes in the dynamic compressive tests.

According to formula (6) and (7), the dynamic force on one side of the specimen P_1 is proportional to the sum of the incident (In) and reflected (Re) stress waves, and the dynamic force on the other side P_2 is proportional to the transmitted (Tr) wave. Figures 10 and 11 show the original and extracted signals in a typical dynamic compressive test, respectively. It can be seen from Fig. 11 that the curve of the sum of the incident and reflected waves almost overlaps with that of the transmitted wave, which indicates that P_1 and P_2 are nearly identical during the dynamic compressive test period. In this condition, the inertial effects are eliminated because there is no global force difference in the specimen to induce inertial forces (Dai and Xia 2010; Huang et al. 2010).

Figure 12 presents the dynamic compressive stress–strain curves of specimens with different water contents. Compared with static compressive tests, the specimens

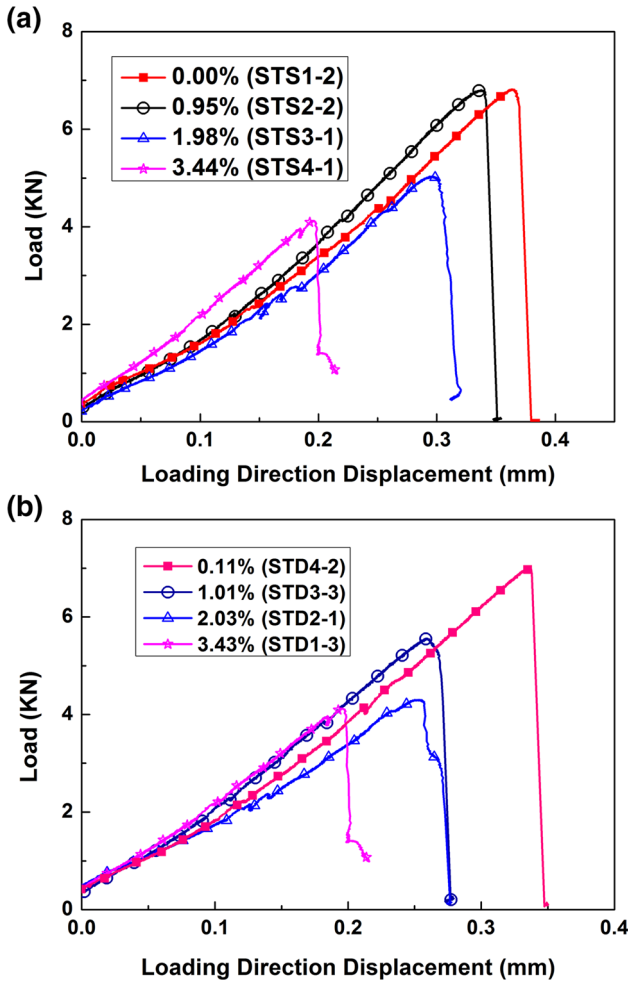

Fig. 7 Load-displacement curves for different water contents. **a** Saturation process; **b** drying process

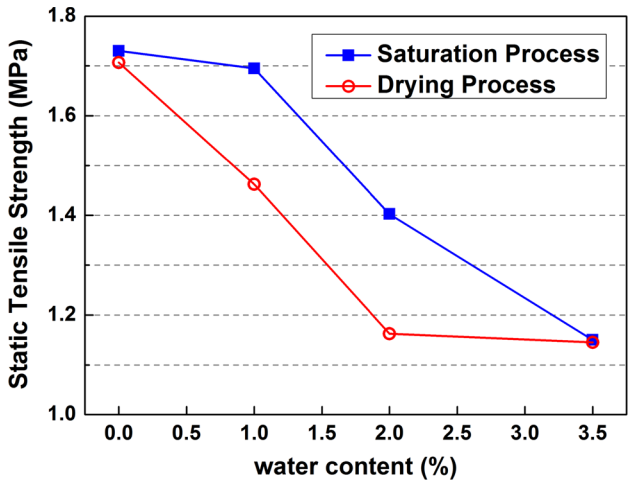

Fig. 8 Variation of static tensile strength versus water content

enter the elastic stage without a compaction stage, which makes the pre-peak region of the stress–strain curve nearly linear. In addition, because of the high loading rate, specimens are destroyed instantaneously. Thus, the dynamic compressive elastic modulus is larger than the static one. Moreover, with the increase of water content, the failure strain and the slope of stress–strain curve at the elastic stage decrease accordingly. At the post-peak stage, the stress of specimens with lower water contents drops more rapidly while that of specimens with higher water contents descends more slowly. This situation also demonstrates that water could weaken the mechanical capability of sandstone even in dynamic situations.

Figure 13 further shows the dynamic compressive strength of specimens with different water contents. The regression analysis also reveals that the relationship between the dynamic compressive strength and water content can be determined using the following equations: In saturation process:

$$\sigma_c(\omega_w) = 51.24 + 35.971e^{-0.576\omega_w} \quad (R^2 = 0.929) \qquad (11)$$

In drying process:

$$\sigma_c(\omega_w) = 52.68 + 33.368e^{-0.585\omega_w} \quad (R^2 = 0.924). \qquad (12)$$

It can be seen that, in the saturation process, when specimens changed from dry state to saturated state, its average dynamic compressive strength reduced from 86.19 to 51.24 MPa, almost a 40.5 % reduction. In the drying process, when the water content declined to 0.08 %, the dynamic compressive strength of the specimen was about 84.80 MPa, which was close to that of dry specimens.

5.3 Dynamic Tensile Properties of Rock With Different Water Contents

Tables 11 and 12 give the parameters of specimens with different water contents from both saturation and drying processes in the dynamic tensile tests.

Figures 14 and 15 show the original and extracted signals in a typical dynamic tensile test, respectively. It can be seen that the signals in tensile tests are different from those in dynamic compressive tests. In dynamic Brazilian tensile tests, specimens usually fail quickly before incident stresses increase to a high level and the most part of the incident wave is reflected into the input bar. Therefore, the transmitted stress wave is very weak. It can also be seen from Fig. 15 that the dynamic force curves on both sides of the BD specimen almost overlap, which again indicates the stress equilibrium of the specimen. In the tensile tests, the

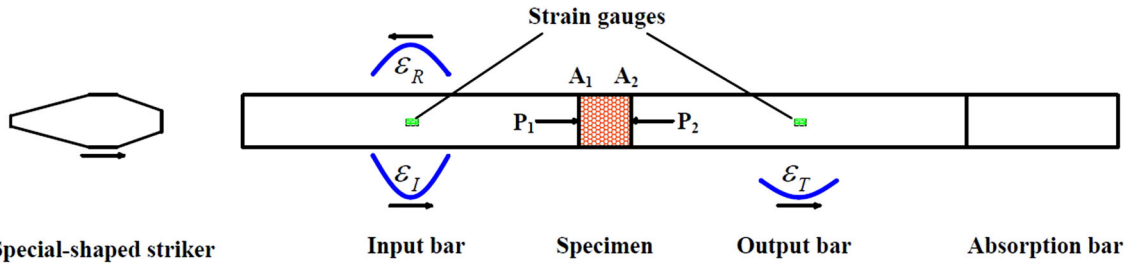

Fig. 9 Configuration of the SHPB system

Table 9 Specimen parameters in dynamic compressive tests (saturation process)

Specimen no.	Water content/%		P-wave velocity/m s^{-1}		Density/kg m^{-3}		Strength/MPa		Strain rate /s^{-1}
	Design	Test	Dry	Wet	Dry	Wet	Tested	Average	
DCS1-1	0.0	0.00	2676.52	–	2338.0	–	83.97	86.19	100.0
DCS1-2		0.00	2717.93	–	2365.9	–	85.42		105.9
DCS1-3		0.00	2728.35	–	2381.4	–	88.15		98.7
DCS1-4		0.00	2768.97	–	2401.1	–	87.23		106.4
DCS2-1	1.0	1.03	2697.24	2697.24	2329.8	2353.8	78.24	73.39	104.0
DCS2-2		1.04	2737.57	2720.57	2331.0	2355.2	69.14		98.6
DCS2-3		1.01	2698.32	2687.49	2348.9	2372.6	70.45		101.1
DCS2-4		0.97	2579.93	2563.9	2342.9	2365.6	75.73		94.0
DCS3-1	2.0	2.04	2660.62	2711.46	2338.2	2385.9	58.07	64.41	107.9
DCS3-2		1.99	2642.08	2745.01	2352.1	2398.9	69.14		109.2
DCS3-3		2.13	2705.31	2792.58	2367.0	2417.4	65.61		111.0
DCS3-4		2.02	2593.01	2711.65	2333.4	2380.5	64.81		98.7
DCS4-1	3.5	3.56	2646.63	3165.58	2337.5	2420.7	54.63	51.24	103.8
DCS4-2		3.37	2645.49	3171.08	2343.8	2422.8	48.81		105.4
DCS4-3		3.41	2620.54	3049.06	2339.1	2418.9	50.29		98.3
DCS4-4		3.44	2741.52	3177.26	2353.3	2434.3	51.22		105.5

dynamic tensile strength can be calculated by the formula (7) directly.

Figure 16 presents the dynamic tensile strength of specimens versus water content. The figure clearly illustrates that the dynamic tensile strength gradually decreases as the water contents of specimens increase in the saturation process. When the specimen was saturated, the dynamic tensile strength reduced to 7.06 MPa, which was almost 72.4 % of that of dry specimens. It can also be seen that when the water content was below 1.0 %, the dynamic tensile strength was almost unchanged.

Figure 16 also presents results in the drying process. It is worthwhile to note that the dynamic tensile strength did not vary significantly with the reduction of water content from 3.5 to 2.0 %. After that, the dynamic tensile strength increased gradually with the decrease of the water content. It also shows that when the water content reduced to 0.16 %, the dynamic tensile strength reached 9.67 MPa and approached that of dry specimens.

Particularly, there is a significant distinction among tensile strength values of specimens with the same water content but in different processes. From Fig. 16 and Tables 11, 12, when the water content was 1.0 %, the dynamic tensile strength value of the specimen in the saturation process was 9.67 MPa, while being 8.02 MPa in the drying process. A difference of 17.1 % can be observed. When the water content was 2.0 %, the dynamic tensile strength values of the specimen in the saturation process and drying process were 8.59 and 7.10 MPa respectively, which yielded a distinct difference of 17.3 %. This indicates that, not only water content but also water distribution would play important roles in controlling the dynamic tensile failure of sandstone rocks.

Table 10 Specimen parameters in dynamic compressive tests (drying process)

Specimen no.	Water content/%		P-wave velocity/m s^{-1}		Density/kg m^{-3}		Strength/MPa		Strain rate $/s^{-1}$
	Design	Test	Dry	Wet	Dry	Wet	Tested	Average	
DCD1-1	3.5	3.45	2651.48	3165.58	2337.5	2418.1	49.58	52.68	101.3
DCD1-2		3.49	2649.45	3171.08	2343.8	2425.6	57.12		98.2
DCD1-3		3.51	2623.15	3049.06	2339.1	2421.2	51.79		104.2
DCD1-4		3.47	2743.32	3177.26	2353.3	2435.0	52.21		99.5
DCD2-1	2.0	2.09	2790.80	2915.24	2326.0	2374.6	63.48	63.47	101.2
DCD2-2		1.93	2790.70	3071.64	2320.5	2365.3	58.09		95.7
DCD2-3		1.99	2786.24	2736.19	2326.5	2372.8	64.34		105.0
DCD2-4		2.04	2717.89	2803.36	2230.5	2276.0	67.96		110.7
DCD3-1	1.0	1.01	2671.16	2654.97	2236.9	2259.5	73.48	74.25	97.0
DCD3-2		0.97	2689.46	2657.06	2242.2	2264.0	76.47		99.0
DCD3-3		1.07	2685.47	2669.20	2234.3	2258.2	77.19		87.3
DCD3-4		1.03	2606.49	2559.66	2226.5	2249.5	69.86		93.9
DCD4-1	0.0	0.13	2585.93	2701.22	2230.8	2233.7	78.73	84.80	105.1
DCD4-2		0.04	2782.38	2881.75	2336.1	2337.1	86.88		94.1
DCD4-3		0.06	2748.06	2826.67	2322.0	2323.4	83.11		98.8
DCD4-4		0.09	2763.87	2678.84	2228.0	2230.0	90.46		101.0

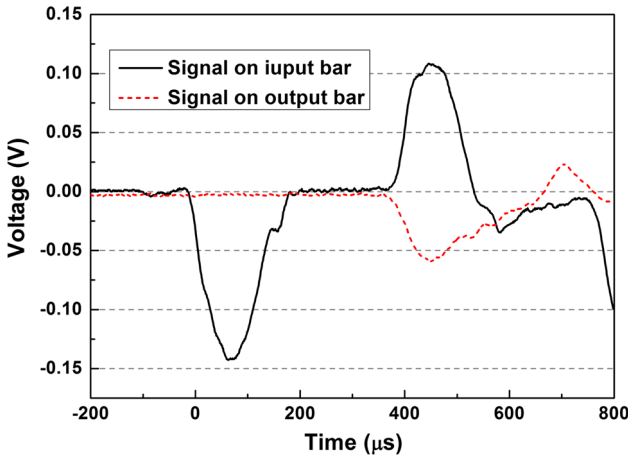

Fig. 10 Original signals in a typical dynamic compressive test

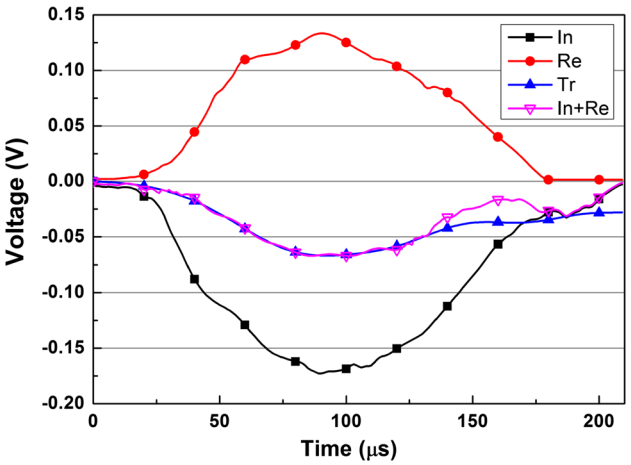

Fig. 11 Extracted signals in a typical dynamic compressive test (*In* incident wave, *Re* reflected wave, *Tr* transmitted wave)

6 Conclusions and Discussion

In this paper, the water distribution in both the saturation and drying processes was obtained from NMR-images. A series of dynamic and static experiments were carried out on sandstone specimens with different water contents during the two processes, and the effect of water content on the mechanical properties of rock was experimentally studied.

From tests, reductions of the compressive and tensile strength of sandstone under static and dynamic states in different saturation processes were observed. There is no generally accepted explanation for the influence of water on rock strength, although several water weakening mechanisms on the strength of rock have been proposed, including pore pressure, chemical and physical deterioration, capillary tension, etc. Some of these factors have been described by Van Eeckhout (1976) and McConnell (1989). In reality, the deformation of wet rocks is usually due to their combined effects. It is obvious that some factors are

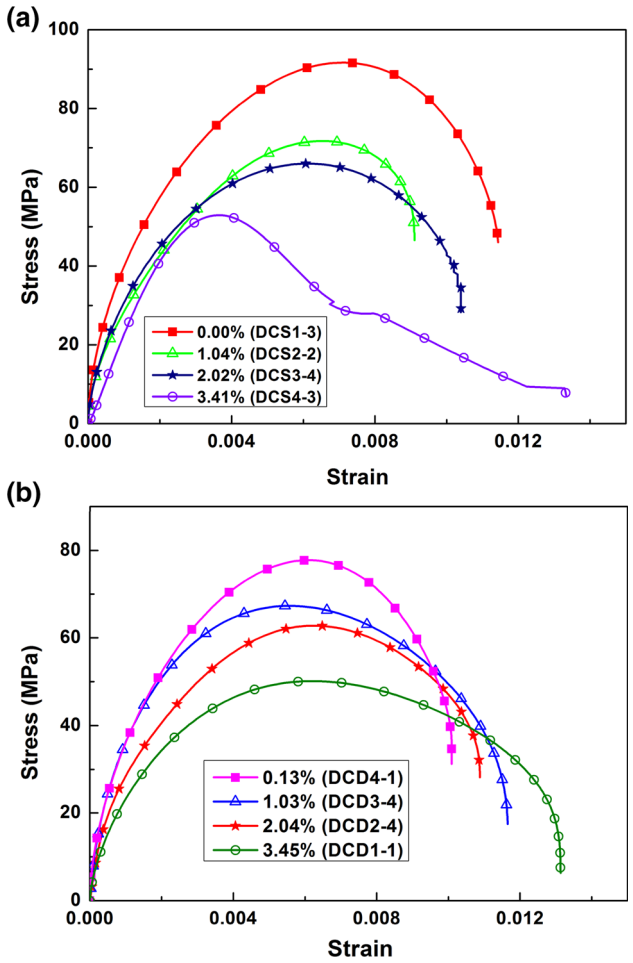

Fig. 12 Dynamic stress–strain curves for different water contents. **a** Saturation process; **b** drying process

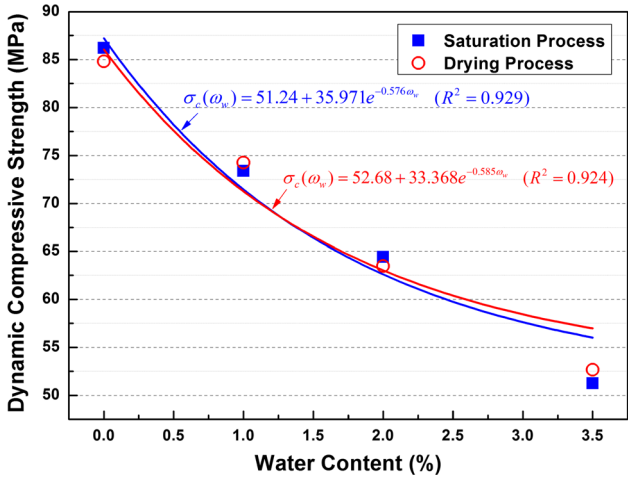

Fig. 13 Variation of dynamic compressive strength versus water content

more significant than others for certain rock types and conditions. With respect to pore pressures, it would be significant when the rock is saturated and pores are fully filled with water. But in this study, the rock strength reduces greatly even when the water content is less than 3.51 %, so it can be concluded that pore pressure plays a limited role in affecting the mechanical properties. As for chemical and physical deterioration, chemical reaction of the hydrolysis of rock minerals usually occurs in a strong chemical environment. The purified water used in the laboratory tests can hardly lead to chemical deterioration. As shown in Table 1, some physical solution and softening might take place as the rock material contains some clay minerals.

Besides the possible pore pressure effect, the water inside the rock may bring into crack splitting tensile force, which further reduces the rock strength in static cases. During the dynamic test, the loading speed is quite fast, and free water inside the rock cannot come out and provide certain carrying capacity. At the same time, the surface tension of free water in wing cracks and the Stefan effect will retard the crack propagation (Rossi 1991). From these points of view, water is beneficial for dynamic strength of rock. However, due to the high strain rate of loading conditions, dynamic cracks expand fast, and water fails to reach the crack tips and the retarding effect of water does not work on the cracks effectively. So with the increase of water content, the dynamic strength still decreases.

From Figs. 8 and 16, significant distinction can be observed for tensile strength values of specimens with the same water content but in different processes, which indicates that the capillary effect may play an important role. This is because the capillary effect is different for capillary spaces during the saturation and drying processes. Meanwhile, Figs. 6 and 13 show that there is no obvious strength difference for rocks under compressive tests in the saturation and drying processes. The reason may come from the different deformation and failure mechanisms of specimens in compressive tests and tensile tests. In compressive tests, the specimen is loaded at both ends and deforms uniformly. When it reaches the peak strength, a large amount of micro-cracks will appear, as shown in Fig. 17a. All the rock skeleton other than certain micro-cracks or moisture will affect the overall strength. In Brazil tensile tests, the specimen is loaded at the diametrical points on the BD disc. Only one or several main cracks can form when the specimen fails, as shown in Fig. 17b. The fracture force of the main cracks controls the mechanical behavior completely. As discussed before, the water is more easily able to exert an influence on the fracture force

Table 11 Specimen parameters in dynamic tensile tests (saturation process)

Specimen no.	Water content/%		P-wave velocity/m s^{-1}		Density/kg m^{-3}		Strength/MPa		Strain rate
	Design	Test	Dry	Wet	Dry	Wet	Tested	Average	
DTS1-1	0.00	0.00	2646.78	–	2346.17	–	9.68	9.75	94.3
DTS1-2		0.00	2689.50	–	2349.18	–	9.97		96.9
DTS1-3		0.00	2723.37	–	2339.54	–	9.68		103.4
DTS1-4		0.00	2562.84	–	2350.99	–	9.67		94.1
DTS2-1	1.00	1.13	2691.38	2658.15	2332.67	2359.03	9.55	9.67	93.6
DTS2-2		1.05	2654.28	2637.79	2348.81	2373.47	9.52		99.5
DTS2-3		1.02	2681.09	2681.09	2333.96	2357.77	9.77		86.8
DTS2-4		0.97	2718.18	2718.18	2360.48	2383.38	9.82		113.0
DTS3-1	2.00	1.99	2753.03	2702.36	2345.90	2392.58	8.84	8.59	104.0
DTS3-2		2.06	2752.27	2804.86	2331.09	2379.11	8.69		98.2
DTS3-3		2.03	2605.65	2689.70	2341.29	2388.82	8.22		107.9
DTS3-4		2.01	2612.86	2679.86	2348.78	2395.99	8.62		97.4
DTS4-1	3.50	3.49	2727.78	3052.06	2328.03	2409.28	7.22	7.06	102.6
DTS4-2		3.46	2782.27	3136.80	2355.25	2436.74	6.84		89.4
DTS4-3		3.40	2789.47	3144.90	2332.57	2411.88	7.17		100.4
DTS4-4		3.53	2695.68	3093.70	2343.74	2426.47	6.99		96.7

Table 12 Specimen parameters in dynamic tensile tests (drying process)

Specimen no.	Water content/%		P-wave velocity/m s^{-1}		Density/kg m^{-3}		Strength/MPa		Strain rate
	Design	Test	Dry	Wet	Dry	Wet	Tested	Average	
DTD1-1	3.5	3.51	2646.63	3165.58	2338.0	2420.1	7.13	7.08	103.3
DTD1-2		3.48	2645.49	3171.08	2365.9	2448.2	7.09		101.8
DTD1-3		3.43	2620.54	3049.06	2381.4	2463.1	7.10		99.7
DTD1-4		3.46	2741.52	3177.26	2401.1	2484.2	6.99		105.2
DTD2-1	2.0	2.06	2575.68	2529.41	2329.8	2377.8	7.19	7.10	96.7
DTD2-2		1.97	2735.42	2752.2	2331.0	2376.9	7.20		110.0
DTD2-3		2.02	2652.65	2718.97	2348.9	2396.3	7.07		106.4
DTD2-4		2.03	2658.95	2762.54	2342.9	2390.5	6.93		106.2
DTD3-1	1.0	1.19	2670.39	2653.8	2338.2	2366.0	8.05	8.02	96.0
DTD3-2		1.06	2647.62	2663.86	2352.1	2377.0	7.89		99.6
DTD3-3		0.98	2672.59	3207.11	2367.0	2390.2	8.14		102.2
DTD3-4		1.04	2661.88	2614.06	2333.4	2357.7	7.98		92.9
DTD4-1	0.0	0.23	2570.94	2554.98	2337.5	2342.9	9.50	9.67	109.4
DTD4-2		0.14	2814.07	2831.76	2343.8	2347.1	10.05		106.2
DTD4-3		0.09	2709.87	2693.45	2339.1	2341.2	9.67		97.2
DTD4-4		0.18	3034.52	3034.52	2353.3	2357.5	9.46		104.7

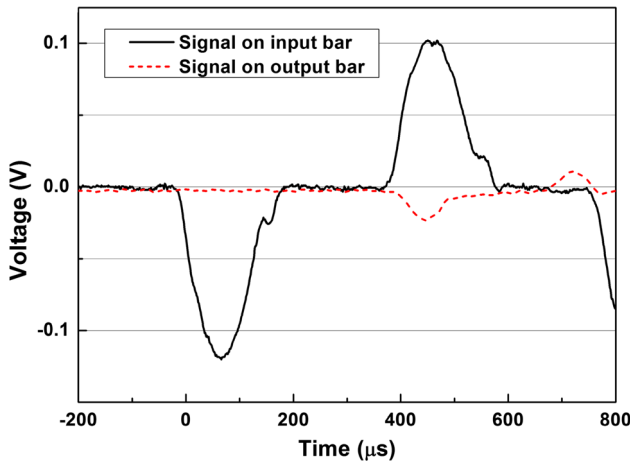

Fig. 14 Original signals in a typical dynamic tensile test

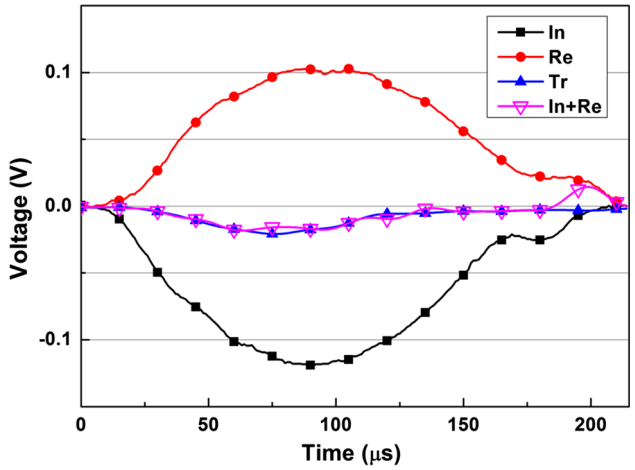

Fig. 15 Extracted signals in a typical dynamic tensile test (*In* incident wave, *Re* reflected wave, *Tr* transmitted wave)

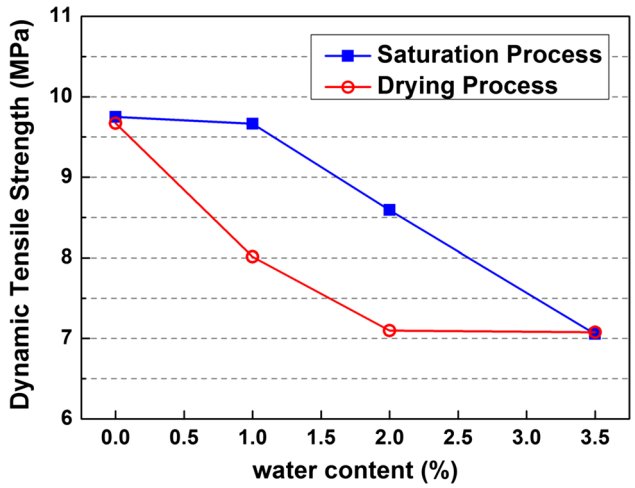

Fig. 16 Variation of dynamic tensile strength versus water content

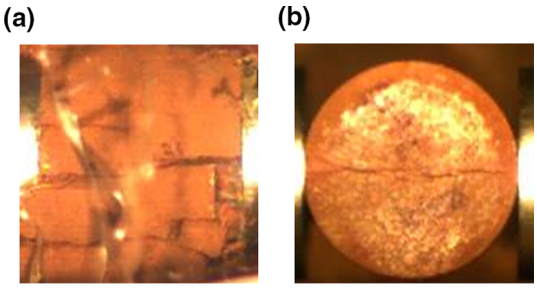

Fig. 17 Different failure patterns of specimens in compressive and tensile tests: **a** failure in compressive test; **b** failure in tensile test

through Stefan effect or capillary effect. And water has different micro-behaviors in the saturation and drying processes. So significant distinction can be observed in the tensile strength values of specimens with the same water content but different water treatment.

Acknowledgments The authors acknowledge the financial support from both the National Natural Science Foundation of China (51322403, 51274254) and National Basic Research Program of China (2015CB060200).

References

Bai H, Ma D, Chen Z (2013) Mechanical behavior of groundwater seepage in karst collapse pillars. Eng Geol 164:101–106

Bieniawski ZT, Hawkes I (1978) Suggested methods for determining tensile strength of rock materials. Int J Rock Mech Min Sci Geomech Abstr 15:99–103

Broch E (1974) The influence of water on some rock properties. Proceeding of the 3rd Congress of the International Society for Rock Mechanics, pp 33–38

Buxton RB (2009) Introduction to functional magnetic resonance imaging: principles and techniques. Cambridge University Press, Cambridge

Colback P, Wild B (1965) The influence of moisture content on the compressive strength of rocks. Proceeding of the 3rd Canadian Symposium on Rock Mechanics, pp 55–83

Dai F, Xia K (2010) Loading rate dependence of tensile strength anisotropy of Barre granite. Pure appl Geophys 167(11):1419–1432

Dai F, Huang S, Xia K, Tan Z (2010) Some fundamental issues in dynamic compression and tension tests of rocks using split Hopkinson pressure bar. Rock Mech Rock Eng 43(6):657–666

Edelman RR, Warach S (1993) Magnetic resonance imaging. N Engl J Med 328(10):708–716

Eeckhout EMV, Peng SS (1975) The effect of humidity on the compliances of coal mine shales. Int J Rock Mech Min Sci Geomech Abstr 12(11):335–340

Hawkins AB, Mcconnell BJ (1992) Sensitivity of sandstone strength and deformability to changes in moisture content. Eng Geol 25(2):115–130

Huang S, Xia K, Yan F, Feng X (2010) An experimental study of the rate dependence of tensile strength softening of Longyou sandstone. Rock Mech Rock Eng 43(6):677–683

Iverson RM (2000) Landslide triggering by rain infiltration. Water Resour Res 36(7):1897–1910

Lu T, Zhao Z, Hu H (2011) Improving the gate road development rate and reducing outburst occurrences using the waterjet technique in high gas content outburst-prone soft coal seam. Int J Rock Mech Min Sci 48(8):1271–1282

McConnell BJ (1989) Factors controlling sandstone strength and deformability in uniaxial compression. University of Bristol

Rossi P (1991) A physical phenomenon which can explain the mechanical behaviour of concrete under high strain rates. Mater Struct 24(6):422–424

Song D, Wang E, Liu Z, Liu X, Shen R (2014) Numerical simulation of rock-burst relief and prevention by water-jet cutting. Int J Rock Mech Min Sci 70:318–331

Van Eeckhout EM (1976) Mechanisms of strength reduction due to moisture in coal mine shales. Int J Rock Mech Min Sci Geomech Abstr 13(2):61–67

Vásárhelyi B (2005) Statistical analysis of the influence of water content on the strength of the Miocene limestone. Rock Mech Rock Eng 38(1):69–76

Vásárhelyi B, Ván P (2006) Influence of water content on the strength of rock. Eng Geol 84(s 1–2):70–74

Zhang QB, Zhao J (2014) A review of dynamic experimental techniques and mechanical behaviour of rock materials. Rock Mech Rock Eng 47(4):1411–1478

Zhou YX, Zhao J (2011) Advances in rock dynamics and applications. CRC Taylor & Francis press, Boca Raton

Zhou Z, Li X, Ye Z, Liu K (2010) Obtaining constitutive relationship for rate-dependent rock in SHPB tests. Rock Mech Rock Eng 43(6):697–706

Zhou J, Chen X, Wu L, Kan X (2011a) Influence of free water content on the compressive mechanical behaviour of cement mortar under high strain rate. Sadhana 36(3):357–369

Zhou Z, Li X, Liu A, Zou Y (2011b) Stress uniformity of split hopkinson pressure bar under half-sine wave loads. Int J Rock Mech Min Sci 48(4):697–701

Zhou YX, Xia K, Li XB, Li HB, Ma GW, Zhao J, Dai F (2012) Suggested methods for determining the dynamic strength parameters and mode-I fracture toughness of rock materials. Int J Rock Mech Min Sci 49:105–112